Diurnal heat balance for the northern Monterey Bay inner shelf

S. H. Suanda,[1] J. A. Barth,[1] and C. B. Woodson[2]

Received 15 December 2010; revised 8 June 2011; accepted 24 June 2011; published 27 September 2011.

[1] In the summer of 2007, physical measurements including velocity from acoustic Doppler current profilers, surface gravity wave heights measured acoustically, and temperature from thermistor chain arrays were collected along- and across- the mid to inner shelf (water depths from 10–60 m) in northern Monterey Bay. The oceanic response to a strong (8–15 m s^{-1} daily maximum) along-shelf sea breeze is examined by evaluating the diurnal heat budget over a cross-shelf section of the inner shelf. The diurnal heat budget closes to within the 95% confidence level with daily warming and cooling periods explained by two separate, but related processes. During evening/early morning warming period, 77% of the observed temperature increase is due to along-shelf advection of a temperature gradient within the upwelling shadow zone, a process which is arrested during the period of wind-forcing. In contrast, 75% of the afternoon cooling period is explained by the cross-shelf heat flux driven by diurnal along-shelf winds. In this study, diurnal tides are found to contribute less than 10% of the observed temperature variability and surface gravity waves do not show any significant diurnal variability. Richardson number estimates show that, on average, wind-induced shear is not strong enough to erode the strength of water column stratification within the upwelling shadow.

Citation: Suanda, S. H., J. A. Barth, and C. B. Woodson (2011), Diurnal heat balance for the northern Monterey Bay inner shelf, *J. Geophys. Res.*, *116*, C09030, doi:10.1029/2010JC006894.

1. Introduction

[2] Monterey Bay is a large semi-circular bay situated in central California. Like much of the west coast of North America, the regional-scale, summer-time oceanic circulation is driven by upwelling-favorable winds. For Monterey Bay, this has been the topic of many studies and is still an active area of research due to the unique and complicating effects of bay geometry and bathymetric features [e.g., *Ramp et al.*, 2005; *Rosenfeld et al.*, 1994, 2009]. During periods of sustained upwelling-favorable winds, the main coastal upwelling center is to the north of the bay at Pt. Año Nuevo [*Rosenfeld et al.*, 1994]. Cold upwelled waters can be seen in satellite imagery traveling across the mouth of Monterey Bay and offshore, isolating bay waters from regional-scale circulation [*Rosenfeld et al.*, 1994; *Paduan and Rosenfeld*, 1996]. Bay waters inshore of the upwelling jet are shielded from regional wind by the Santa Cruz mountains, and form a counter-clockwise rotating, recirculation zone in the northern part of the bay. This region is characterized by a 5–10 m surface layer of warm water termed the 'upwelling shadow,' which sits above cold, subsurface, recently upwelled water [e.g., *Rosenfeld et al.*, 1994; *Graham and Largier*, 1997; *Ramp et al.*, 2005]. Similar embayment-wide circulation features have also been documented in other upwelling regions such as the Chilean coast [*Marín et al.*, 2001].

[3] Upwelling shadow zones are of interest because their physical characteristics typically deviate from classical two-dimensional coastal upwelling and they are often also regions of increased biological activity [e.g., *Graham and Largier*, 1997; *Marín et al.*, 2001]. This paper focuses on diurnal-period temperature fluctuations at the northern end of the Monterey Bay upwelling shadow (Figure 1a). In contrast to the northerly upwelling winds that characterize regional-scale wind-forcing, during active upwelling periods the wind-forcing on the northern Monterey Bay shelf is primarily due to a local sea breeze [*Banta*, 1995; *Drake et al.*, 2005]. Here the coastline orientation is parallel to the dominant direction of the sea breeze and these along-shelf winds drive diurnal upwelling, a source of cold water to the inner shelf [*Woodson et al.*, 2007]. Diurnal-period dynamics within the study area are further complicated by the behavior of a sharp front between warm shadow waters and the cold upwelling jet which propagates poleward along-shelf as a buoyancy driven, coastally-trapped plume [*Woodson et al.*, 2009].

[4] Hourly time series of local winds, water column temperature, and currents from this region all show a strong diurnal signal (Figure 2). The correlation between these variables has been previously noted in the literature where the cooling of inner-shelf waters occurs during flow that is both eastward (into Monterey Bay) and onshore at depth, while the opposite circulation patterns are observed during warming [*Rosman et al.*, 2007]. On the diurnal scale, water column cooling occurs during midday, when solar insulation is at its

[1] College of Oceanic and Atmospheric Sciences, Oregon State University, Corvallis, Oregon, USA.
[2] Environmental Fluid Mechanics Laboratory, Stanford University, Stanford, California, USA.

0148-0227/11/2010JC006894

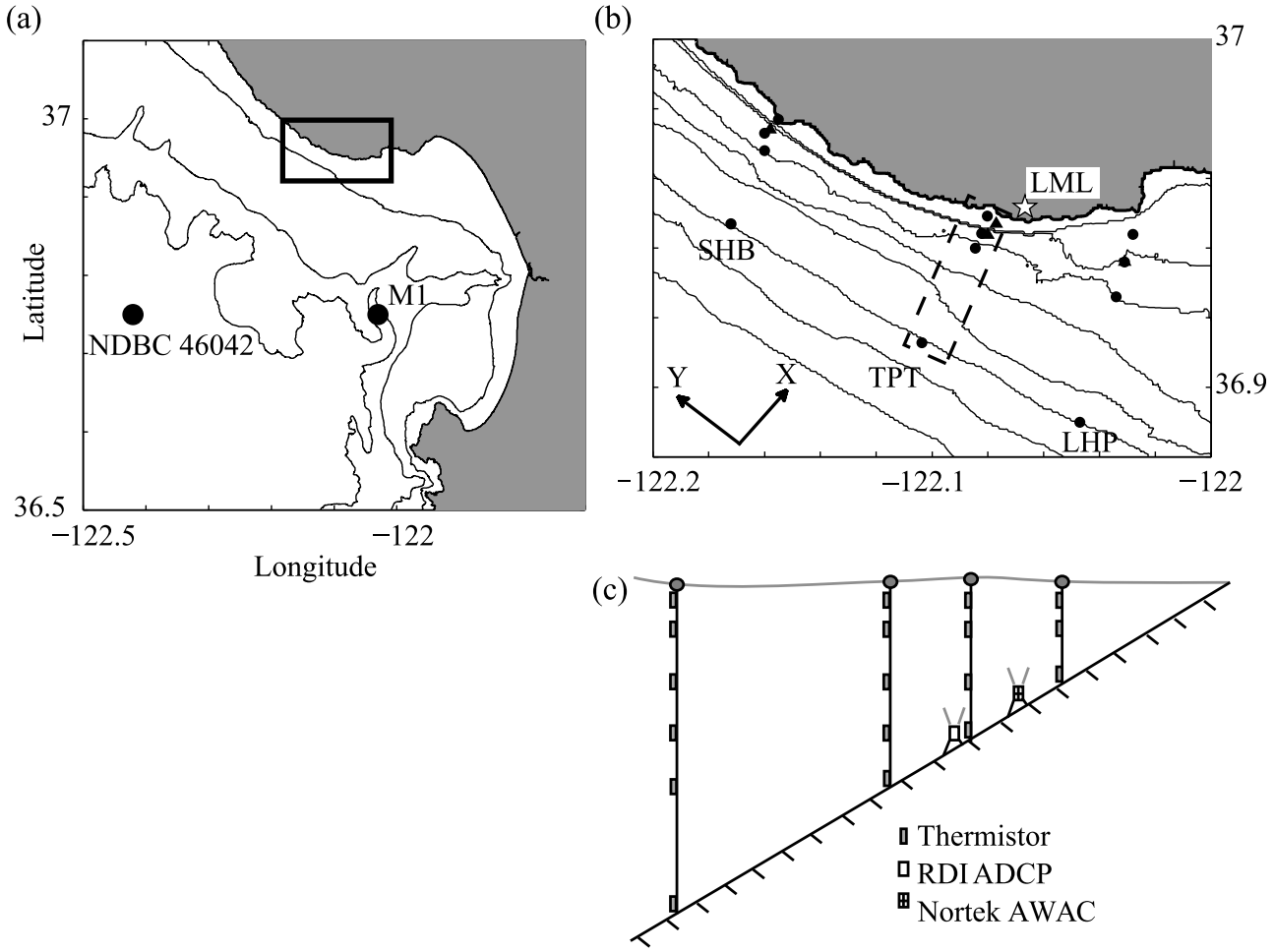

Figure 1. (a) Map of Monterey Bay showing location of offshore wind station NOAA NDBC buoy 46042 and meteorological buoy MBARI M1. The black square denotes the study location. (b) Close-up of inner-shelf study region. Bathymetry is shown in 10-m increments along with thermistor chains (circles) and acoustic current profiler (triangles) locations. Also noted is the location of UCSC Long Marine Laboratory (star). (c) Cross-shelf view of thermistor and current profiler array off of Terrace Point (TPT).

peak [*Woodson et al.*, 2007]. The analysis here aims to build on these previous works to isolate the forcing mechanism of diurnal temperature fluctuations. This is done by creating a canonical day picture of the variables that is phase-locked to the sea breeze and then evaluating terms in the heat budget of a two-dimensional cross-shelf section of the inner shelf.

[5] Sea breeze-driven, diurnal-period coastal temperature fluctuations have been previously explored off the Chilean coast [*Kaplan et al.*, 2003]. *Kaplan et al.* [2003] showed the stratifying effect of daytime heating and river runoff competes with the destabilizing effect of wind-driven shear to determine the observed diurnal temperature changes at two coastal locations. In northern Monterey Bay, the upwelling shadow provides the source of stratification [*Woodson et al.*, 2007]. In this study, the role of mixing within the cross-shelf section is assessed by the Richardson number as the potential contribution of mixing holds different consequences for the physical (e.g., maintenance of upwelling shadow) and biological understanding of the northern Monterey Bay inner shelf.

[6] Previous studies of coastal upwelling and downwelling have used water velocity and temperature data to estimate terms in the heat budget written for different geometrical configurations [e.g., *Lentz*, 1987; *Send et al.*, 1987; *Dever and Lentz*, 1994; *Austin*, 1999]. These studies have focused on both fluctuating and mean subtidal heat budgets, uncovered dominant balances within the budget, and increased understanding of the forcing mechanisms. *Lentz* [1987] derived a conservation equation for the heat content of a three-dimensional volume in the Coastal Ocean Dynamics Experiment (CODE) region (centered on 38.5°N, 123.5°W) during the summer upwelling season and was able to close both the mean and subtidal heat budget with observational data. *Lentz* [1987] found good agreement between measured offshore heat flux and a two-dimensional Ekman model across the control volume. For spring and winter, *Dever and Lentz* [1994] estimated the heat balance for a two-dimensional cross-shelf slice. The mean balance during spring was similar to the summer as in the work of *Lentz* [1987], but the mean winter balance was three-dimensional.

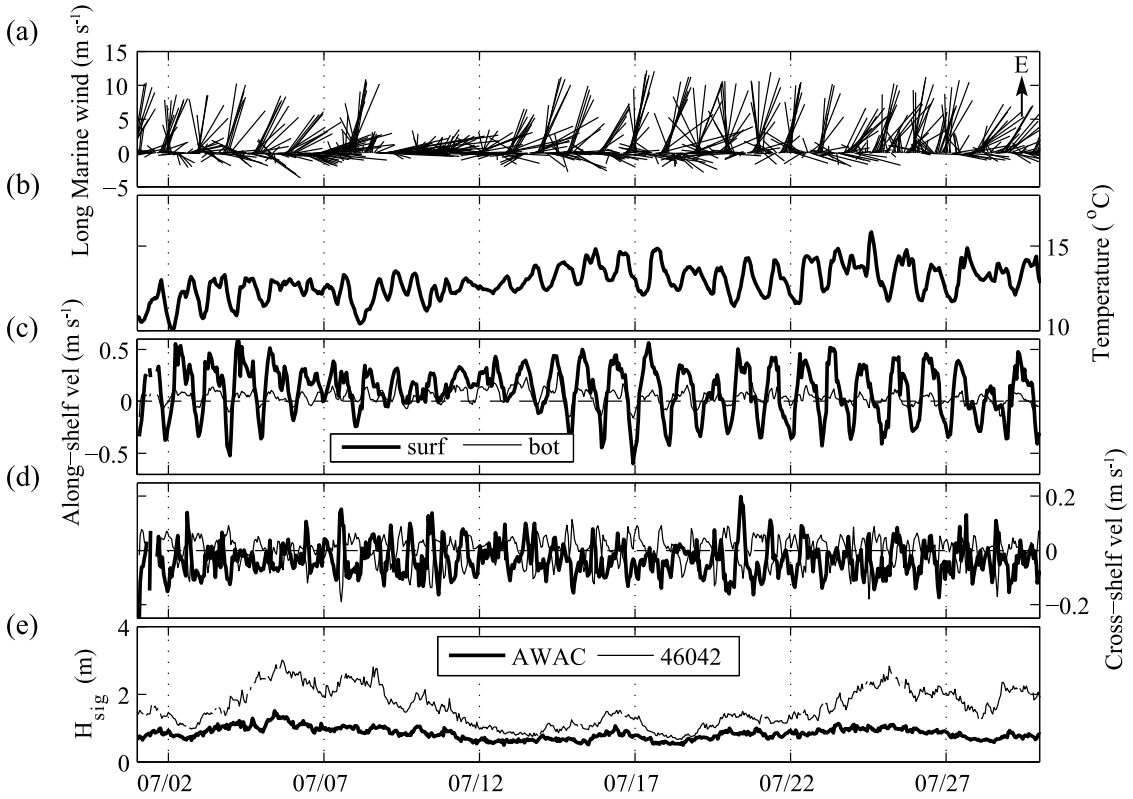

Figure 2. Hourly averaged time series of variables from July 2007: (a) Local vector winds from Long Marine Laboratory. (b) Average water column temperature at Terrace Point 20-m. (c) Surface (thick black) and bottom (thin grey) along-shelf currents. (d) Surface (thick black) and bottom (thin grey) cross-shelf currents. (e) Significant wave height measured at NDBC buoy 46042 (thin grey) and at AWAC (thick black).

Subtidal fluctuations during both seasons showed the dominance of the cross-shelf heat flux in determining water column temperature [*Dever and Lentz*, 1994]. Focusing on a two-dimensional slice of the inner-shelf of North Carolina, *Austin* [1999] showed that the relationship between along-shelf wind and heat content depends on water column stratification, thus switching sign seasonally throughout the year.

[7] The remainder of the paper is organized as follows. Section 2 describes the field site, data gathered, and analysis methods used in this work. Section 3 presents the results of the mean and diurnal heat budget as well as Richardson number and diurnal Ekman transport calculations. Section 4 is a discussion of the results and section 5 provides a summary and describes potential biological implications from the findings of this study.

2. Methods

2.1. Field Site and Data

[8] The northern Monterey Bay inner shelf is relatively straight, oriented east-west and contains both sand and rocky substrates. The rocky areas are seasonally covered by kelp forest which stretch from offshore (~15 m depth) to the edge of the surf zone [*Rosman et al.*, 2007]. Data used are from 15 May to 15 August 2007 during a larger study in northern Monterey Bay conducted by the Partnership for Interdisciplinary Studies of Coastal Oceans (PISCO) [*Woodson et al.*, 2009]. Water column velocity and temperature data are from a series of mid- to inner-shelf arrays shown in Figure 1. The PISCO study instrumented a 15-km stretch of the northern Monterey Bay shelf and included moorings, Acrobat tows, and biological sampling. This paper focuses on data from the moorings placed in cross-shelf arrays at the 10-, 20-, 30-, and 60-m isobaths off Sand Hill Bluff (SHB), Terrace Point (TPT), and Light House Point (LHP). On each mooring, temperature loggers (Stowaway Tidbits, Onset, Inc.) recorded temperature at two- or four-minute intervals [*Woodson et al.*, 2009]. These data were run through a three standard deviation filter and bin-averaged into hourly time series.

[9] At the three cross-shelf array locations, a bottom-mounted Acoustic Doppler Current Profiler (ADCP; RDI Workhorse 600 kHz, Teledyne Inc.) was deployed at the 20-m isobath. The ADCPs recorded 45 pings per two-minute ensemble averaged into 1-m bins. To minimize near-surface data loss due to sidelobe reflection, a "tide-following" processing method is adopted following *Kirincich et al.* [2005]. Backscatter intensity from the 4 beams are added together and the maximum value is taken as the surface. All velocity data above and 10% below this level are discarded. Extrapolation of velocity profiles to the surface and bottom (data is missing due to signal blanking) are needed to estimate the total transport through the water column. For each profile, velocity is linearly extrapolated from the value at the deepest good ADCP bin to a no-slip condition of zero velocity at the ocean

Table 1. Location, Type, Acoustic Frequency, and Principal Axes of Current Meters Used in This Study

Location	Type	Principal Axes Between Major Axes and True North
SHB (20 m)	RDI Workhorse 600 KHz	322°
TPT (20 m)	RDI Workhorse 600 KHz	294°
TPT (15 m)	Nortek AWAC 1 MHz	278°
LHP (20 m)	RDI Workhorse 600 KHz	276°

bottom and velocity at the shallowest bin is extrapolated at a constant value to the surface position. Other extrapolation methods to the surface and bottom were compared and yielded similar results. Extrapolated current profiles were then bin averaged to hourly values.

[10] Measured water column velocities from all current profilers are rotated into the principal axes as defined by hourly depth-averaged values (Table 1). Once rotated, currents were assumed to be in the along- (cross-) shelf direction for the major (minor) axes. In the following analysis, the coordinate system is defined such that the positive y-axis is along-shelf toward the north pole and the x-axis is positive onshore with zero at the coast.

[11] In addition to the 20-m ADCP, from 29 June–30 July 2007, an Acoustic Wave and Current Profiler (AWAC; Nortek 1 MHz) was deployed at the 15-m isobath along the TPT line. In addition to velocity profiles, measurement of the sea surface with 2-Hz Acoustic Surface Tracking (AST) combined with wave orbital velocity measurements allowed the AWAC to resolve the surface gravity wave directional spectrum.

[12] Meteorological data are taken from a variety of sources to complement in situ measurements. Regional winds are taken from NOAA NDBC buoy 46042. In addition, local wind data are taken from UCSC Long Marine Lab, less than two kilometers from the TPT inner-shelf array. As no measurements of surface heat flux were available locally, measured solar radiation variables are from the M1 meteorological buoy located in the middle of Monterey Bay (Figure 1a), 20 km to the south of the study area. Due to data gaps in a few of the temperature records, only the period when concurrent temperature, current, and meteorological data are available is used (1 June–9 August, 2007).

2.2. Creating the Canonical Day

[13] To quantify the diurnal cycle of circulation and temperature structure on the inner shelf, a canonical day is created by computing the average hourly value for all variables during the summer study period. Previous work has established a strong relationship between diurnal wind and water column temperature fluctuations at this location [*Woodson et al.*, 2007], so to isolate variability in relation to the diurnal wind, the averaging is phase-locked to the sea breeze cycle. Over the 2.5 months when all data are available, there are 45 days where local westerly sea breeze reached a maximum of at least 8 m s^{-1}. A composite average is created for these days by taking hourly values of wind, temperature and water column velocity, and averaging in time centered on the peak of the westerly wind. Each of the 12 hours leading to and following maximum wind are also averaged, thus forming a picture of the canonical wind-forced day.

2.3. Heat Budget Equation

[14] Following previous studies [e.g., *Dever and Lentz*, 1994; *Austin*, 1999], the heat equation is written for a two-dimensional cross-shelf slice in the cross-shelf and vertical directions (x, z). This area is bounded in the vertical by the ocean bottom, $z = -H(x)$, and the surface, $z = 0$. In the cross-shelf direction it is bounded by the 20-m isobath offshore, $x = -L$ (1150 m), and the coast, $x = 0$ (Figure 3). Combining the equations for conservation of a tracer (temperature) and continuity gives the heat budget for this area

$$\rho c_p \int_{-L}^{0}\int_{-H}^{0} \frac{\partial T}{\partial t} dz dx = \rho c_p \left[\int_{-H}^{0} uT|_{x=-L} dz - \int_{-L}^{0}\int_{-H}^{0} \cdot \left(T\frac{\partial v}{\partial y} + v\frac{\partial T}{\partial y} \right) dz dx \right] + \int_{-L}^{0} Q_o dx. \quad (1)$$

Here T is the water temperature, u and v are horizontal velocities in the x (cross-shelf) and y (along-shelf) directions, respectively, Q_o is the net air-sea heat flux where positive (negative) values indicate a heating (cooling) of the ocean by the atmosphere, ρ is the density of seawater (1025 kg/m^3) and c_p is the specific heat (3993J/kgC). Equation (1) states that heat fluxes into and out of the two-dimensional slice change the heat content within this control volume (left-hand side of equation (1)). Beginning with the first term on the right-hand side, these fluxes are the cross-shelf heat flux at the offshore side of the volume, along-shelf heat flux due to volume flux divergence and temperature gradient flux, and the net surface heat flux (Figure 3).

[15] In order to use the continuity relation to simplify (1), temperature and cross-shelf velocity components are decomposed into vertical average and perturbation quantities ($u = \langle u \rangle + u'$and $T = \langle T \rangle + T'$; where $\langle u \rangle = H^{-1} \int_{-H}^{0} u|_{x=-L} dz$

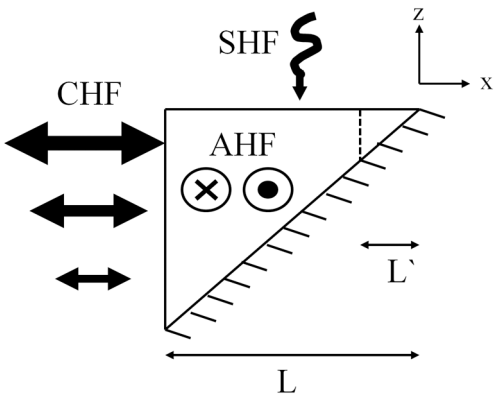

Figure 3. Schematic of terms in the heat budget for the two-dimensional coastal slice: Cross-shelf heat flux (CHF), along-shelf heat flux (AHF), and surface heat flux (SHF). Also noted are the length of the control volume from its offshore side to the coast (L) and the length by which the control volume is reduced (L′).

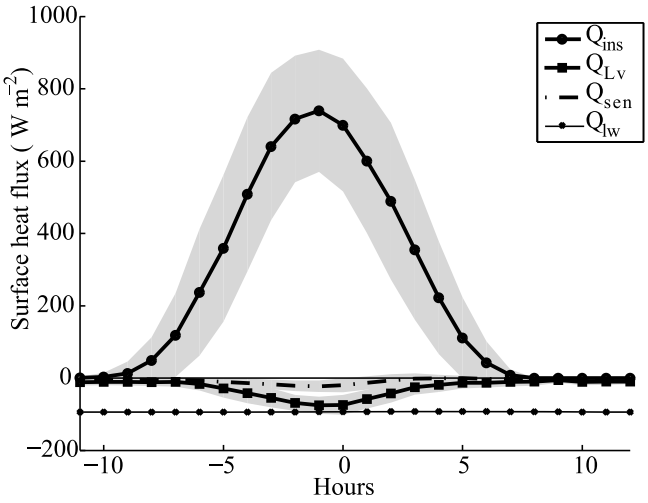

Figure 4. Individual terms in the diurnal surface heat flux. Positive values represent heat transferred from the atmosphere to the ocean. Shaded areas represent one standard deviation from the mean.

and $\langle T \rangle = H^{-1} \int_{-H}^{0} T|_{x=-L} dz$) such that the first term on the right-hand side of (1) becomes

$$\int_{-H}^{0} uT|_{x=-L} dz = \langle u \rangle \langle T \rangle H + \int_{-H}^{0} u'T'dz|_{x=-L}. \tag{2}$$

Assuming along-shelf velocity is constant in the cross-shelf direction, temperature is decomposed into area average and perturbation quantities ($T = \overline{T} + T'$; where $\overline{T} = A^{-1} \int_{-L}^{0} \int_{-H}^{0} T dz dx$). The second term on the right-hand side of (1) becomes

$$\begin{aligned}\int_{-L}^{0}\int_{-H}^{0}\left(T\frac{\partial v}{\partial y} + v\frac{\partial T}{\partial y}\right)dzdx = \overline{T}\int_{-L}^{0}\int_{-H}^{0}\frac{\partial v}{\partial y}dzdx \\ + \int_{-L}^{0}\int_{-H}^{0} T'\frac{\partial v}{\partial y}dzdx \\ + \int_{-L}^{0}\int_{-H}^{0} v\frac{\partial T}{\partial y}dzdx.\end{aligned} \tag{3}$$

By continuity, the first term on the right-hand side of (2) will cancel the first term on the right-hand side of (3) if the vertically averaged temperature on the offshore side of the volume is equivalent to the area averaged temperature ($\langle T \rangle = \overline{T}$). These two values are within one standard deviation of each other through the canonical day (see Appendix). The second term is difficult to estimate without knowledge of the form of $\partial v/\partial y$ variations across the control volume and will be neglected in the following analysis. The potential errors introduced by these assumptions are discussed in the Appendix.

[16] With these simplifications and with the assumption that the surface heat flux is constant across the control volume, (1) can be rewritten;

$$\begin{aligned}\rho c_p \int_{-L}^{0}\int_{-H}^{0}\frac{\partial T}{\partial t}dzdx = \rho c_p \int_{-H(-L)}^{0} u'T'dz|_{x=-L} \\ - \rho c_p \int_{-L}^{0}\int_{-H}^{0} v\frac{\partial T}{\partial y}dzdx + Q_o L.\end{aligned} \tag{4}$$

This equation is similar to *Dever and Lentz* [1994, equation 1] and *Austin* [1999, equation 1]. The term on the left-hand side of the equality sign represents the change in heat stored in the two-dimensional coastal slice (HS). On the right-hand side the terms are the cross-shelf heat flux (CHF), along-shelf heat flux (AHF), and surface heat flux (SHF), respectively. These various terms can be estimated from the temperature and current data gathered during the PISCO experiment and the heat budget closes if a balance is achieved between the measured heat change (HS) and the sum of the three terms on the right-hand side of (4). The main assumption made in this derivation has been that of along-shelf velocity uniformity in the cross-shelf direction ($v \neq v(x)$). This assumption cannot be identically true as along-shelf velocity must fulfill a no slip condition at or near the coast. The effect of a simple form of $v(x)$ is considered in section 4.

2.4. Estimating Terms From Data

[17] To estimate these terms from data, trapezoidal integration is performed on the time-mean and individual hour of the canonical day temperature and current fields. Temperature loggers were not evenly distributed in the vertical and cross-shelf directions, thus to estimate the amount of heat stored in the volume these measurements are weighted by the area defined as half the distance to adjacent instruments or to an integration limit. The sum of the weights is equal to the area of the two-dimensional coastal slice. For cross-shelf heat flux, deviations from depth-average velocity (u') are multiplied by deviations from the vertically averaged temperature (T') at the offshore side and integrated from the bottom to the surface. Temperature measurements were not as finely resolved in the vertical as ADCP velocity bins and are interpolated to the same grid as ADCP velocity measurements before integrating. Temperature profiles obtained with this method are comparable to Acrobat and CTD profiles collected during the experiment [*Woodson et al.*, 2009]. Along-shelf heat flux is estimated by multiplying measured along-shelf velocity (v) by the along-shelf temperature gradient ($\partial T/\partial y$) at TPT defined by a centered difference of temperature from SHB to LHP at each logger's position within the control volume, and then integrating across the volume with the same weighting scheme as the heat storage estimate.

[18] Surface heat flux is estimated as the sum of its various terms multiplied by the length of the shelf. It consists of the sum of incoming solar radiation, latent, sensible heating, and losses due to long wave radiation:

$$Q_o = Q_{ins} + Q_{Lv} + Q_{sen} + Q_{lw} \tag{5}$$

When the sum is positive (negative), heat is being input to (removed from) the ocean's surface. Canonical day surface heat flux terms are calculated using bulk formulas following *Rosenfeld et al.* [1994] (Figure 4). The time base in Figure 4 is in canonical day hours, and shows total surface heat flux to be dominated by incoming solar radiation, which peaks 2 hours prior to maximum wind (around noon local time).

2.5. Diurnal Ekman Transport

[19] This calculation compares measured surface transports to a theoretical wind-driven Ekman transport. Though the methodology is similar to *Lentz* [2001] and *Kirincich et al.*

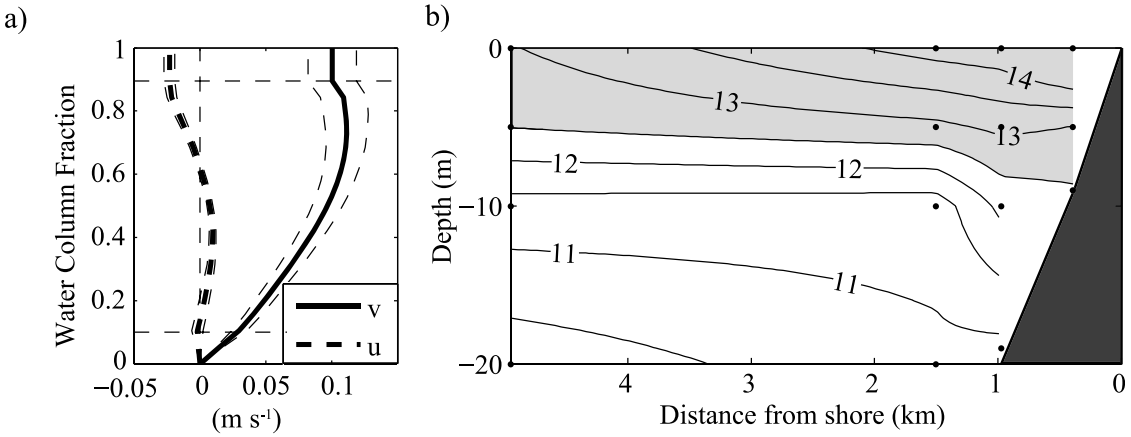

Figure 5. Time-mean plots of: (a) Along-shelf (v) and cross-shelf (u) velocity profiles with one standard error from the mean shown as dashed lines. The horizontal dashed lines mark the extrapolated section of the profiles. (b) Time-mean temperature contour of the upper 20-m of the inner shelf at Terrace Point. The temperature contour of 12.5° and warmer are shaded to represent the approximate location of Monterey Bay upwelling shadow.

[2005] which study subinertial variability, a large percentage of wind speed and current variance in northern Monterey Bay is explained by the diurnal band and thus results here are interpreted as diurnal Ekman transports. To estimate both measured and theoretical transports, wind and velocity data are low-pass filtered using a Cosine-Lanczos filter with a 20-hr cutoff [*Mooers*, 1968]. A depth-averaged velocity is removed from ADCP cross-shelf velocity profiles and then surface-extrapolated as described previously. The profile is then integrated from its first zero crossing to the surface, thus defining a surface transport. This measured transport is compared to a theoretical value for Ekman transport ($\tau/\rho f$) by neutral regression, whose slope is interpreted as a percent of realized theoretical transport.

3. Results

[20] Monthlong time series of wind vectors, water column temperature, along-shelf and across-shelf velocities, and significant wave height are shown in Figure 2. Except for significant wave height, these data show strong diurnal fluctuations in all variables. Local wind-forcing (Figure 2a) shows a sea-breeze pattern where diurnal winds blow toward the east, in the along-shelf direction, and reach magnitudes of 10 m s^{-1} during midday [*Woodson et al.*, 2007]. Time series of significant wave height (Figure 2e) shows waves at Terrace Point are smaller than those observed offshore, consistent with the sheltering effect northern Monterey Bay experiences from summertime northern swell.

[21] Before examining the diurnal motions, it is useful to first consider the time-mean behavior of currents and water column temperatures at Terrace Point across the full 2.5 month data record (Figure 5). The mean along-shelf velocity is directed northwestward out of Monterey Bay throughout the water column, while the cross-shelf velocity shows a sheared water column with offshore flow at the surface and onshore flow at depth. Both of these are consistent with mean spring/summer season profiles from a previous study [*Drake et al.*, 2005]. The mean cross-shelf temperature section of the upper 20-m shows the warm upwelling shadow (denoted here as waters warmer than 12.5°C) sitting above the colder background water. The various terms in the time-mean heat budget can also be calculated (Table 2). While the mean surface heat flux and along-shelf heat flux contribute heat to the control volume, the mean cross-shelf heat flux works to remove heat. To within a standard deviation, the total sum of the mean heat fluxes balances the mean variation in heat storage, which is small (Table 2).

[22] A summary of canonical day wind, currents, and average inner-shelf temperature is shown in Figure 6. The time base in these plots is ordered relative to the peak in the westerly winds (approximately 2 pm local time) and daily cycles for each variable are evident. Westerly winds begin to blow in the late morning (−7 hrs) and intensify over an 8-hour period (Figure 6a). The wind peaks at 10 m s^{-1} then dies down at a similar rate and remains calm overnight. The average water column temperature (Figure 6b), taken as the average of all thermistors in the inner-shelf array, shows a 12 hour period of temperature decrease beginning at the start of the westerly winds, followed by a warming period (7 hrs) during weak winds.

[23] The variation of currents with depth shows the along- and cross-shelf current response to this wind. Along-shelf currents (Figure 6c) flow out of the bay for most of the day, consistent with pressure gradient and buoyancy-driven poleward flow at the northern end of the upwelling shadow [*Drake et al.*, 2005; *Woodson et al.*, 2009]. Daily-averaged surface and depth-averaged along-shelf velocities are 0.09 m s^{-1} and 0.08 m s^{-1}, respectively. As the wind

Table 2. Time-Mean Values and Standard Errors of Heat Flux Terms[a]

Heat Equation Term	Mean	Standard Error
Surface Heat Flux (SHF)	1.06	0.28
Cross-shelf Heat Flux (CHF)	−8.15	1.96
Along-shelf Heat Flux (AHF)	9.23	1.78
Total Heat Flux:	2.14	2.97
Heat Storage (HS):	0.01	4.87

[a]Units are in 10^5 W m^{-1}.

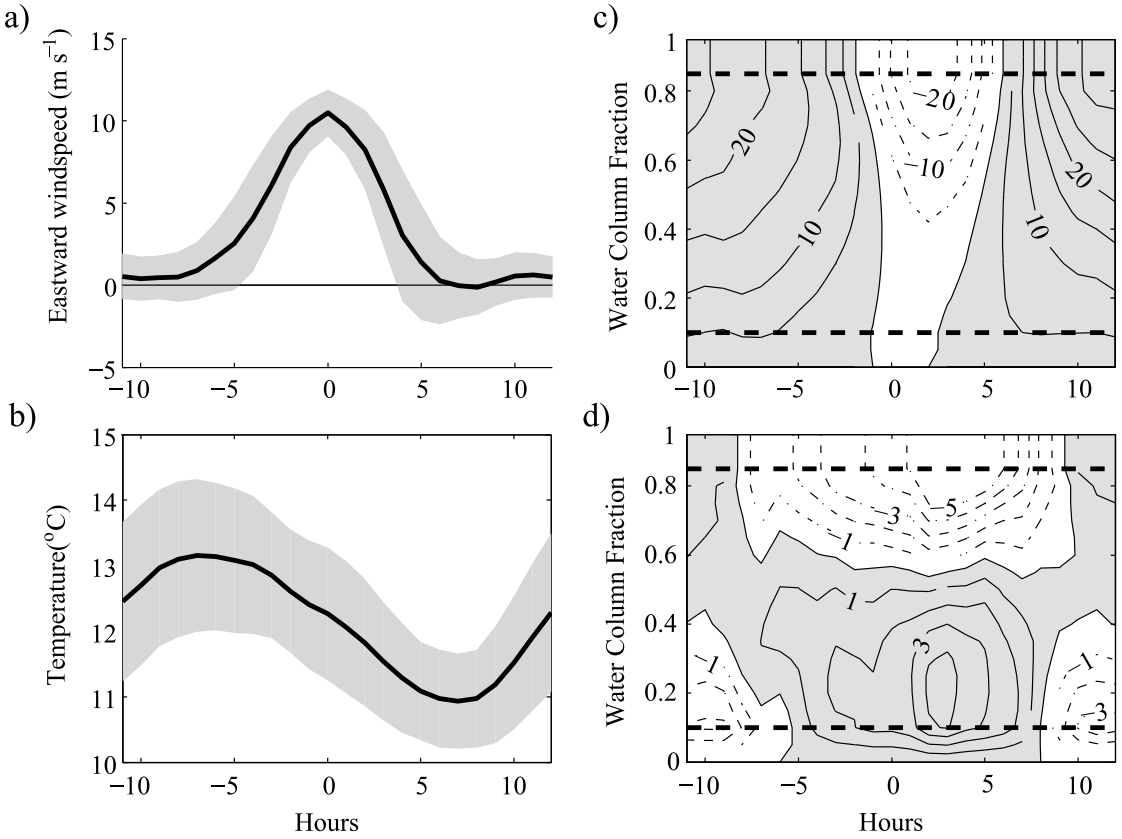

Figure 6. Canonical day plots of: (a) Westerly winds. Shaded areas represent one standard deviation from the mean. (b) Average inner-shelf temperature. Along- (c) and cross-shelf (d) current measured at Terrace Point (TPT) 20-m isobath. In Figures 6c and 6d, contour labels are in (cm s^{-1}), positive values are shaded and horizontal dashed lines mark the extrapolated section of the profiles.

builds, surface currents first decrease in intensity and then reverse to flow downwind. Near maximum wind (0 hrs), flow throughout the entire water column is directed downwind (into the bay) reaching peak surface speeds of 0.23 m s^{-1}. This persists for 2 hours when near-bottom currents return to flow out of the bay while surface currents remain directed downwind until the sea breeze relaxes and along-shelf flow throughout the water column returns to its background state. Overall, flow is weaker in the cross-shelf direction (Figure 6d). Prior to wind-forcing (before −6 hrs), surface currents are weakly onshore with offshore flow at depth. During the period of wind-forcing, surface currents become directed offshore (toward negative x-axis) with opposing onshore flow at depth. The zero crossing in this sheared profile is a little higher than half of the water column and the flows reach maximum velocities of −0.08 m s^{-1} (0.04 m s^{-1}) in the surface (bottom) at 4 hours after maximum wind. As the wind relaxes, surface currents return to weakly onshore with corresponding offshore flow at depth.

[24] TPT cross-shelf temperature structure in the upper water column (<20-m depth) in the canonical day is shown as cross-shelf temperature sections (Figure 7). Again, temperatures above 12.5°C are shaded to illustrate the upwelling shadow water mass which resides across the shelf (−11 hrs to −3 hrs). Except for an isolated surface signature at the 10-m mooring, between −1 hrs and 3 hrs these warm waters are removed from this cross-section and beginning at −3 hrs, colder water fills in below the shadow. Toward the end of the sea breeze forcing (5 hrs to 9 hrs), warm water reappears across the study region.

[25] Using the canonical day values of temperature, velocity, and surface heat flux, the various terms on the right-hand side of the heat conservation equation (4) are estimated. Surface heat flux (SHF) is positive and warms the water column, though it generally has a smaller effect than the other two terms (Figure 8a). The cross-shelf heat flux (CHF) is primarily negative (cooling) with brief periods when it warms the control volume (−11 to −8 hrs and 9 to 12 hrs). Along-shelf heat flux (AHF) shows mostly a warming pattern, with a short period of cooling during midday (−1 to 5 hrs). To examine whether sources or sinks of heat are missing, heat budget closure is tested by comparing the sum of the three terms on the right-hand side with the estimated heat content change (HS) (Figure 8b). Except for a brief period preceding maximum wind (−3 to −2 hrs), the two estimates are within one standard deviation of each other.

[26] The near-sinusoidal form of the observed daily heat content allows for creation of a longer time series by repeating the cycle (Figures 8c and 8d). The three heat equation terms that can be directly estimated from the data are integrated in time during the warming and cooling periods respectively and compared with the total change in heat content. Starting integration times are chosen based on the sign of the change in heat content (HS). Between −7 hrs and

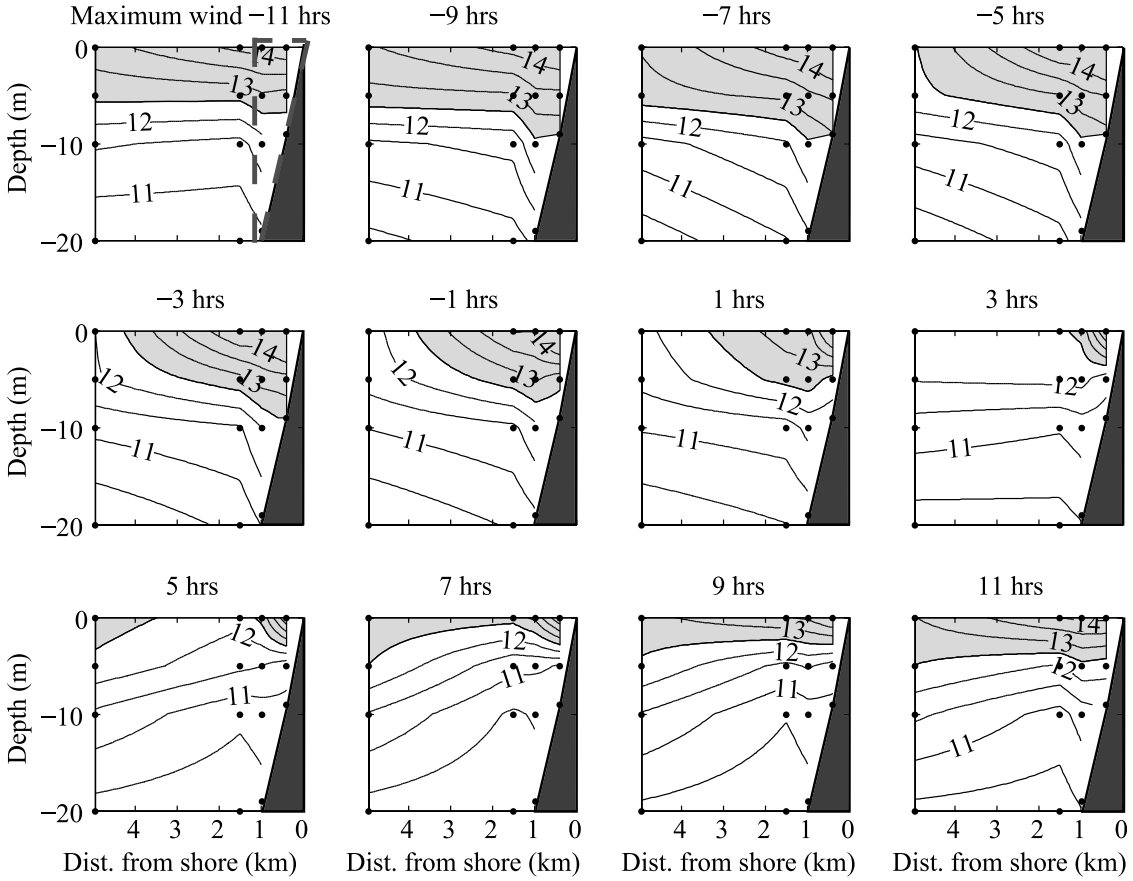

Figure 7. Contour plots of cross-shelf temperature structure at different hours of the canonical day. Measurement locations are indicated by filled circles. The temperature contour of 12.5° and warmer are shaded to represent the approximate location of Monterey Bay upwelling shadow. The dashed triangle in the top left plot shows the control volume for which the diurnal heat budget is evaluated.

7 hrs, HS is negative and represents the period of cooling. Those 14 hours are contrasted with the remaining 10 hours of the day when HS is positive and represents warming. Linear regression is then used to compare each integrated term with the observed warming and cooling (Table 3). These slopes give the percentage of the change in heat that is explained by each term. The total warming period is well-explained by the sum of the estimated terms (95 ± 4%) with along-shelf heat flux dominating the warming (77 ± 3%). During cooling, cross-shelf heat flux is the dominant term (75 ± 2%), however the heat budget does not close as well during this period (67 ± 8%).

[27] The control volume in this calculation extends from the coast (where the cross-shelf heat flux is zero) to the 20-m isobath. However, the location where cross-shelf heat flux terminates could be offshore of the coastline. For example, the surf zone is often considered to consist of a uniform density fluid ($T' = 0$), and in this region along-shelf winds would not drive cross-shelf velocities. By moving the location of this no heat flux condition away from the coast (from $x = 0$ to $x = -L'$), the length of the two-dimensional control volume decreases. This modifies both the total heat contained in the volume and the contributions from the various heat budget terms. The heat budget closes to within 95% confidence level for both periods when the control volume extends from the 20-m isobath to a distance 300 m from the coast ($L' = 300\ m$) (Table 4). Assuming a linear bottom slope, the depth at this location would be about 5 m, a reasonable value for the water depth offshore of the surf zone, but still within the patches of kelp prevalent in the Terrace Point area [*Rosman et al.*, 2007].

[28] Canonical day currents and temperatures are used to calculate the Richardson number, which provides a comparison of stratification (as given by the squared Brunt-Väisälä frequency, $N^2 = -g/\rho_o \partial\rho/\partial z$) to current shear:

$$Ri = \frac{N^2}{\left[\left(\frac{\partial u}{\partial z}\right)^2 + \left(\frac{\partial v}{\partial z}\right)^2\right]} \tag{6}$$

With the location of temperature sensors at 0-, 5-, 10-, and 19-m, estimates of the Richardson number can be given at three depths (Figure 9). These show that for most of the day, the water column is stable to shear-driven mixing (Ri > 0.25) allowing the upwelling shadow to persist through the period of strong wind-forcing. However, in the upper and middle portions of the water column the percent of sub-critical Richardson numbers (Ri < 0.25) increases following the period of maximum wind. In the upper water column (2.5-m depth), shear remains fairly constant throughout the day with a small increase after maximum wind (4 hrs).

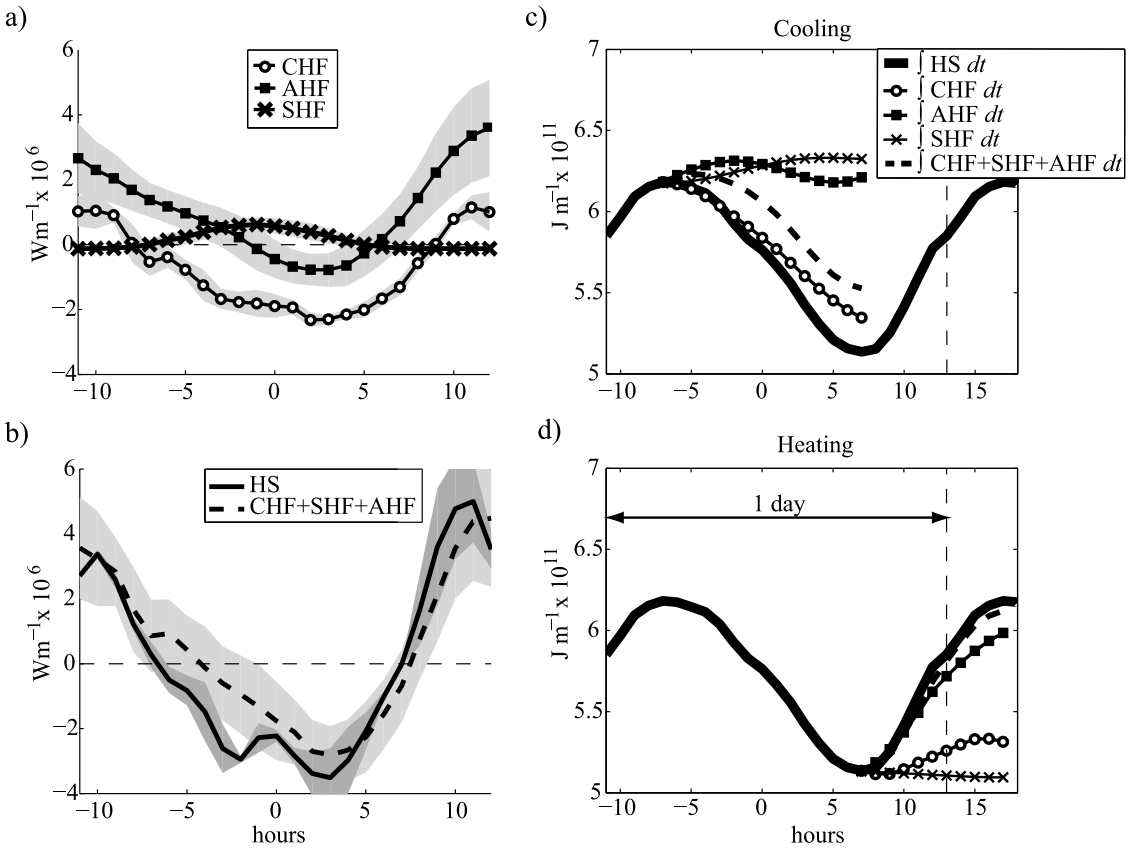

Figure 8. (a) Estimates of 3 terms on the right-hand side of the heat equation (equation (4)): Surface heat flux (SHF), cross-shelf heat flux (CHF), and along-shelf heat flux (AHF). Shaded areas represent one standard deviation from the mean. (b) Comparison of the right-hand and left-hand sides of the heat equation. Dashed line is the sum of three terms on the right-hand side and the solid line is the total change of heat in the control volume (HS). (c) Estimated terms in the heat budget time-integrated during the cooling period (−7 hrs to 7 hrs). (d) Estimated terms in the heat budget time-integrated during the warming period (7 hrs to −7(5) hrs).

Stratification begins to decrease about two hours before maximum wind (−2 hrs) and remains low until the end of wind-forcing (5 hrs). The 20–40% of subcritical Richardson numbers at this time is thus due to a combination of increased wind-driven shear, and decreased surface stratification due to the removal of warm surface water by the cross-shelf heat flux and delivery of cooler water by the along-shelf heat flux. In the later hours (5–10 hrs), stratification increases as along-shelf heat flux returns warm waters to the mooring, and the water column restabilizes. In the middle of the water column, the daily development of the Richardson number is slightly different. Stratification remains fairly constant while current shear increases around the peak in the wind (0–5 hrs) consistent with the location of maximum shear in the cross-shelf velocity profile. The increase in shear allows for destabilization of the mid-water column, promoting active mixing here.

[29] The percentages of realized theoretical surface Ekman transport calculated following the methodology of *Lentz* [2001] and *Kirincich et al.* [2005] are 76 ± 10% (20 m) and 36 ± 8% (15 m) for the two sites in this study (Figure 10). These values are within the error bars found for low-frequency (low-pass filtered with a 40-hr cutoff) Ekman transport at the same depths (15–20 m) in previous studies. This result is discussed below as it is not obvious that diurnal

Table 3. Linear Regression Slope of Each Term in Heat Equation Compared to Total Observed Heat Change[a]

Heat Equation Term	Warming	Cooling
SHF	−3 ± 1%	−15 ± 3%
CHF	21 ± 3%	75 ± 2%
AHF	77 ± 3%	7 ± 6%
Total explained	95 ± 4%	67 ± 8%

[a]Error bars are the 95% confidence levels of the slope estimates.

Table 4. Percentages of Heating and Cooling Explained Along With 95% Confidence Levels for Different Lengths of the Control Volume Slice[a]

L′(m)	L - L′(m)	H(m)	Warming	Cooling
0	1150	0	95 ± 4%	67 ± 8%
100	1050	1.7	97 ± 4%	75 ± 8%
200	950	3.5	100 ± 4%	84 ± 7%
300	850	5.2	103 ± 5%	96 ± 7%

[a]The first row covers the entire length from the coast to the 20-m isobath.

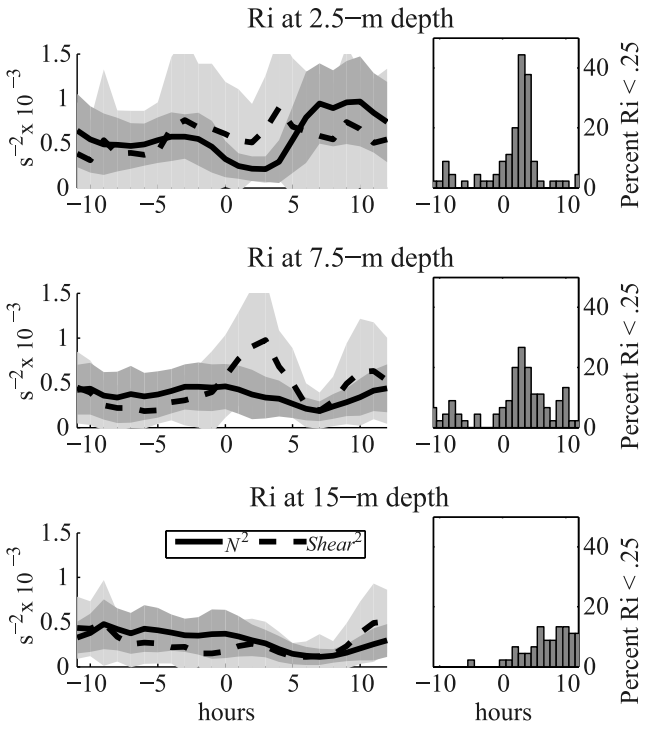

Figure 9. The two components of the Richardson number (buoyancy frequency, N^2 (solid line) and squared velocity shear, $\frac{\partial u^2}{\partial z} + \frac{\partial v^2}{\partial z}$ (dashed line)) estimated at each canonical day hour for three depths in the water column (2.5-m, 7.5-m, and 15-m). The accompanying bar graphs are the percentage of hours from all 45 days used to make the canonical day, where the Richardson number is subcritical (<0.25).

Ekman transport estimates should be comparable to low-frequency estimates.

4. Discussion

[30] Diurnal along- and cross-shelf motions in northern Monterey Bay are sea breeze-driven [*Woodson et al.*, 2007] and coincide with water column temperature changes [*Rosman et al.*, 2007]. Individual terms in the heat budget for a two-dimensional slice of the inner shelf are evaluated with data from an array of current and temperature measurements and two separate terms are identified that explain the majority of diurnal temperature variations. The cooling period is driven primarily by cross-shelf heat exchange, that is an onshore advection of subsurface cold water via upwelling driven by the diurnal wind. The warming period is driven primarily by the along-shelf advection of the temperature gradient between the upwelling shadow and the recently upwelled, cold waters at the mouth of Monterey Bay. Together, these two periods describe the sequence of daily events experienced by the 'upwelling shadow' in this location. During the afternoon sea breeze, the inner shelf is ventilated by subsurface water as a portion of the shadow moves offshore. Richardson number estimates from this period show that, for the most part, wind-driven shears do not erode the stratification provided by the shadow. As the wind subsides, its presence is reinstated less by an onshore return of the shadow, and more due to advection of shadow waters to the east, within northern Monterey Bay.

[31] Based on the percent of total heat change explained, heat budget closure is better achieved during the warming as opposed to the cooling portion of the day (Table 3), and shortening of the control volume achieves nearly 100% closure for both periods (Table 4). Another way to modify the heat budget is to consider different functional forms of along-shelf velocity attenuation across the control volume. For example, previous observations show that kelp forests in this location reduce along-shelf velocities [*Rosman et al.*, 2007]. Here, an along-shelf velocity that linearly decreases from its value at the 20-m isobath to zero at the coast is considered. While the cross-shelf heat flux is not modified by this, the along-shelf heat flux may be significantly affected (see Appendix for details). While previous studies also did not include the effect of cross-shelf non-uniformity in the along-shelf velocity [e.g., *Dever and Lentz*, 1994; *Austin*, 1999], it might be important over the last few inshore kilometers of the shelf studied here. The true effect of a cross-shelf varying along-shelf velocity on the heat budget is difficult to estimate without further knowledge of velocity attenuation across the inner shelf.

[32] We now turn our attention to possible driving mechanisms of the heat fluxes. Measurements of surface gravity waves are potentially relevant as diurnal variations in wave height might drive observed currents that contribute to the heat flux. In fact, the strong afternoon sea-breeze in Monterey Bay has been shown to create significant wind waves and diurnal currents in other portions of the bay [*Hendrickson and MacMahan*, 2009]. When averaged as the other variables, neither significant waves nor wind wave energy (defined here as energy in 2–8 s waves) show a consistent afternoon increase in this location, thus it seems unlikely that the diurnal heat fluxes would be wave-driven.

[33] Though the averaging described above is centered on the sea-breeze cycle, diurnal tides are retained in the canonical day water column velocity and temperature signals. Diurnal tidal removal in both variables is difficult with traditional harmonic analysis because of signal contamination by the strong diurnal wind [e.g., *Rosenfeld et al.*, 2009]. Instead, the maximum contribution of diurnal tides is estimated by prescribing a modeled tidal velocity to advect the

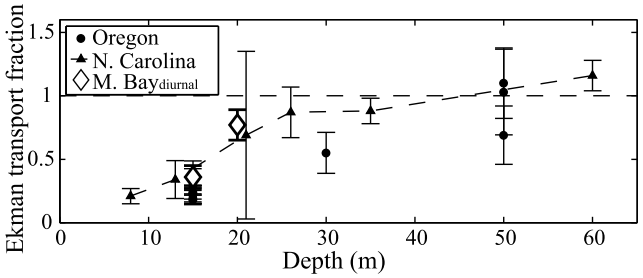

Figure 10. Fraction of the full theoretical Ekman transport at a variety of inner-shelf locations including their 95% confidence levels. Figure reproduced from *Kirincich et al.* [2005], following *Lentz* [2001]. Estimates of the fraction of theoretical diurnal Ekman transport, computed using 20-hr low-pass filtered data, from this study are indicated by diamonds.

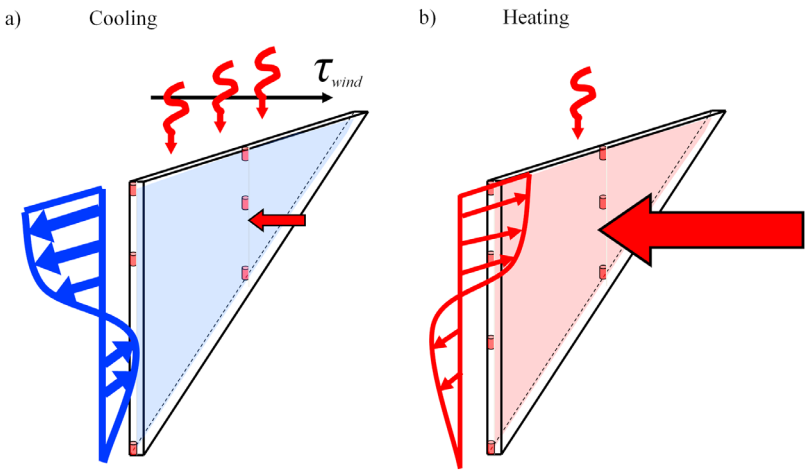

Figure 11. Schematic diagrams illustrating the dominant terms responsible for daily (a) cooling during westerly diurnal winds (black arrow) and (b) warming: surface heat flux (red, squiggly arrows), cross-shelf heat flux (vertical profile with red and blue arrows) and along-shelf heat flux (horizontal red arrows).

canonical day temperature gradients. As the depth-averaged cross-shelf velocity is small (<1 cm s^{-1}), the tidal contribution to heat flux in this direction is neglected. In the along-shelf, the maximum impact of diurnal tides is estimated by using the amplitude of depth-averaged M_2 (12.42 hr) velocity (0.035 m s^{-1}) from T_TIDE harmonic analysis [*Pawlowicz et al.*, 2002], a best fit to the canonical day velocities for tidal phase, which then advects canonical day along-shelf temperature gradients at each level in the water column. This gives the maximum possible contribution from tidal advection as the effect of M_2 astronomical tides should be larger than the diurnal ones in this location and phase has also been locked to the sea breeze. With this estimate, diurnal tides can contribute a maximum of 10% percent of the along-shelf warming/cooling and the majority of the forcing is thus due to other causes.

[34] The analysis here shows the importance of along-shelf temperature gradient advection in warming the water column. The driving force of the northward flow responsible for diurnal water column warming has been identified as a pressure-gradient driven poleward flow that is modified by the sea breeze [*Drake et al.*, 2005; *Woodson et al.*, 2009]. Despite overall smaller velocities, cross-shelf motions drive a heat flux that explains the majority of diurnal cooling of the water column. What mechanism drives these cross-shelf currents? As the sea breeze is predominantly in the along-shelf direction, *Woodson et al.* [2007] show that offshore Ekman transport drives the cross-shelf flow.

[35] Previous studies focused on the inner-shelf response to low frequency (periods > 40 hour) along-shelf winds [*Lentz*, 2001; *Kirincich et al.*, 2005]. Ekman's original theory assumes a steady balance between the Coriolis force and turbulent stress divergence. A scaling of the time-dependent Ekman balance gives the amount of time to reach steady state to be one inertial period divided by π (for this latitude $T_i/\pi \approx$ 6 hours). The results in this study suggest one of two things. Either the spin up of the surface Ekman layer occurs within the time of sea breeze wind-forcing (~10 hours) and steady Ekman dynamics are a good approximation, or it is more appropriate to compare offshore transports driven by periodic forced oscillations to a different quantity than given by steady Ekman dynamics ($U_{ek} = \tau/\rho f$). A simple 1.5 layer model driven by oscillatory surface forcing [*Cushman-Roisin*, 1994] shows the potential for a resonant response to near-inertial forcing, perhaps explaining the high percentage of theoretical Ekman transport observed at 20 m (~75%) at the latitude of Monterey Bay (37°N). Another potential influence on Ekman transport percentages is to consider the effects of background current shear [*Niiler*, 1969]. With this model, the background shear induces an effective Coriolis frequency that modifies the theoretical Ekman transport dependent on the sign of the relative vorticity ($\partial V/\partial x$):

$$U_{ek} = \frac{\tau}{\rho\left(f + \frac{\partial V}{\partial x}\right)} \tag{7}$$

For the northern Monterey Bay case, the horizontal shear that arises from assuming measured low-frequency, westward, along-shelf flow goes to zero at the coast gives a negative relative vorticity which increases U_{ek}. The ratio of measured transport to U_{ek} would then decrease, and perhaps bring the percentages to within the range found in previous studies. The details of this shear-influenced Ekman transport model, or a 1.5 layer model to the shallow inner shelf requires further modeling effort.

5. Conclusions

[36] Here we have examined the diurnal heat budget for a two-dimensional section across the inner shelf of northern Monterey Bay. The study region is in a frontal zone which separates a cold coastal upwelling water mass offshore from the warmer waters of a retentive upwelling shadow near the coast. In coastal upwelling zones, the overall temperature dynamics of embayments such as Monterey Bay involve complex interactions in three spatial dimensions. This is demonstrated by the importance of both along- and cross-shelf motions with vertical structure in the mean and diurnal

heat budget. However, each phase of diurnal temperature change is dominated by one process that occurs in two spatial dimensions, along- and cross-shelf for warming periods, and cross-shelf and vertical for cooling periods as summarized in Figure 11. The advantage of two-dimensionality is that it encourages the use of simple analytical and numerical models, and helps to optimize the placement of instruments to further study and understand the fundamental processes driving these observed flows.

[37] The PISCO study focused on understanding physical processes that could affect the transport and recruitment of intertidal invertebrates and nearshore fish. Results here provide possibilities for how diurnal wind-driven physical processes can affect the transport and delivery of larvae through observed circulation patterns. During the early morning/evening warming period, the system is dominated by along-shelf transport from the shadow zone toward the upwelling plume. Organisms within the shadow would thus experience northwestward along-shelf transport and potentially reach the nose of the upwelling shadow front. *Woodson et al.* [2009] hypothesize that onshore flows occurring in the surface layer near this front can result in shoreward transport for larvae that maintain their position high in the water column. During the afternoon cooling period, the cross-shelf velocity structure is highly sheared with surface waters moving offshore and onshore currents at depth. Through this, organisms that maintain their position in the lower water column can be transported to the coast while those that remain higher in the water column will move offshore and join the larger recirculation pattern of the region. Thus, on a daily timescale material is transported onshore alternately in the surface layer during morning/evening and in the bottom layer during the afternoon.

Appendix A: Sources of Error

[38] Signals estimated from observational data come with associated uncertainty due to measurement error and/or the difference between methods used to derive a particular quantity. At its maximum measurement error, each temperature measurement with a Stowaway logger has an error of 0.4°C due to instrument inaccuracy. The configuration of the RDI ADCP gives a velocity uncertainty of 0.5 cm s^{-1} for each 2-minute ensemble and both hourly and ensemble averaging decreases the uncertainty by sqrt$(N)^{-1}$, where N is the number of samples in the average (30 for hourly averaging; 45 for canonical day averaging). A further source of error comes from determining the principal axis of rotation using depth-averaged currents. A 2° difference in principal axis is found if low-pass filtered depth-averaged currents are used instead of the hourly values used here. While the major axis velocities (along-shelf) are not significantly affected by this, it results in a 20% uncertainty in the cross-shelf velocities.

[39] There are also uncertainties that result from assumptions made in deriving the heat budget equation. The first is due to potential volume flux divergences which arise from neglect of the second term in (3) (a depth-dependent flux divergence) as well as any differences between the vertical average temperature at the offshore side of the control volume ($\langle T \rangle$) and the area average temperature ($\overline{T}$) used to take advantage of continuity. The two average temperatures are within one standard deviation of each other (a maximum difference of 0.4°C), and thus contributes relatively little uncertainty compared with the contribution from the vertical average cross-shelf velocity ($\langle u \rangle$) whose uncertainty is comparable to its magnitude. Ignoring the depth-dependent flux divergence also does not appear to be a large oversight as both the sign and magnitude of along-shelf heat flux contribute to closing the heat budget to 95% confidence without this term.

[40] Another source of uncertainty is from the assumption of cross-shelf uniformity in along-shelf velocity. As in the discussion, a form of along-shelf velocity which decreases linearly to zero at the coast from its measured value 1.15 km offshore potentially impacts the along-shelf heat flux. Without assuming cross-shelf uniformity, (3) is modified because both velocity and temperature have area-average and perturbation contributions ($v = \overline{v} + v'$; where $\overline{v} = A^{-1} \int_{-L}^{0} \int_{-H}^{0} v dz dx$):

$$\int_{-L}^{0}\int_{-H}^{0}\left(T\frac{\partial v}{\partial y}+v\frac{\partial T}{\partial y}\right)dzdx = \int_{-L}^{0}\int_{-H}^{0}\left(T'\frac{\partial v'}{\partial y}+\overline{T}\frac{\partial \overline{v}}{\partial y}+v'\frac{\partial T'}{\partial y}+\overline{v}\frac{\partial \overline{T}}{\partial y}\right)dzdx. \quad \text{(A1)}$$

As previously, using continuity allows the second term on the right-hand side to cancel with the first term in (2). Using estimates based on the data, the perturbation temperature gradient advection (the third term) is about 10% of the mean temperature gradient advection (the last term) and the combination of these two terms can give up to an apparent 50% decrease in along-shelf temperature gradient advection. However, as in (3) and (A1), along-shelf heat fluxes are caused by both temperature gradient advection ($v\partial T/\partial y$) as well as volume flux divergences ($T\partial v/\partial y$). The perturbation volume flux divergence (the first term) has an unknown structure and cannot be quantified with the present data. As this term can potentially be important for a given form of along-shelf velocity attenuation, it is difficult to estimate the true reduction and/or uncertainty in along-shelf heat flux due to the assumption of cross-shelf uniformity.

[41] Lastly, there are errors in the estimate of surface heat flux in Northern Monterey Bay. Due to lack of measurement, cloud cover is ignored in the calculation of outgoing longwave radiation. Errors may also arise from using measurements of incoming solar radiation, relative humidity, atmospheric pressure, and air temperature measured 20 km from the study site, as meteorological fields are known to vary across Monterey Bay during upwelling periods [*Ramp et al.*, 2005]. Without local measurements of these variables, it is difficult to quantify the contribution of this to the total uncertainty.

[42] **Acknowledgments.** This is contribution 398 from PISCO, the Partnership for Interdisciplinary Studies of Coastal Oceans, funded primarily by the Gordon and Betty Moore Foundation and David and Lucile Packard Foundation. We would like to thank Libe Washburn and Margaret McManus for their contributions as well as the PISCO summer field team for their efforts in collecting the data used in this study. We also thank Olivia Cheriton and Fred Bahr for providing data access from UCSC Long Marine Laboratory and MBARI moorings, respectively. This manuscript greatly benefited from suggestions by Libe Washburn, Kate Adams, and two anonymous reviewers.

References

Austin, J. A. (1999), The role of the alongshore wind stress in the heat budget of the North Carolina inner shelf, *J. Geophys. Res.*, *104*(C8), 18,187–18,203.

Banta, R. M. (1995), Sea breezes shallow and deep on the California coast, *Mon. Weather Rev.*, *123*(12), 3614–3622.

Cushman-Roisin, B. (1994), *Introduction to Geophysical Fluid Dynamics*, 320 pp., Prentice-Hall, Upper Saddle River, N. J.

Dever, E. P., and S. J. Lentz (1994), Heat and salt balances over the northern California shelf in winter and spring, *J. Geophys. Res.*, *99*(C8), 16,001–16,017.

Drake, P. T., M. A. McManus, and C. D. Storlazzi (2005), Local wind forcing of the Monterey Bay area inner shelf, *Cont. Shelf Res.*, *25*(3), 397–417.

Graham, W. M., and J. L. Largier (1997), Upwelling shadows as nearshore retention sites: The example of northern Monterey Bay, *Cont. Shelf Res.*, *17*(5), 509–532.

Hendrickson, J., and J. MacMahan (2009), Diurnal sea breeze effects on inner-shelf cross-shore exchange, *Cont. Shelf Res.*, *29*(18), 2195–2206.

Kaplan, D. M., J. L. Largier, S. Navarrete, R. Guiñez, and J. C. Castilla (2003), Large diurnal temperature fluctuations in the nearshore water column, *Estuarine Coastal Shelf Sci.*, *57*(3), 385–398.

Kirincich, A. R., J. A. Barth, B. A. Grantham, B. A. Menge, and J. Lubchenco (2005), Wind-driven inner-shelf circulation off central Oregon during summer, *J. Geophys. Res.*, *110*, C10S03, doi:10.1029/2004JC002611.

Lentz, S. J. (1987), A heat budget for the northern California shelf during CODE 2, *J. Geophys. Res.*, *92*(C13), 14,491–14,509.

Lentz, S. J. (2001), The influence of stratification on the wind-driven cross-shelf circulation over the North Carolina shelf, *J. Phys. Oceanogr.*, *31*(9), 2749–2760.

Marín, V. H., R. Escribano, L. E. Delgado, G. Olivares, and P. Hidalgo (2001), Nearshore circulation in a coastal upwelling site off the northern Humboldt Current System, *Cont. Shelf Res.*, *21*(13–14), 1317–1329.

Mooers, C. N. K. (1968), A compilation of observations from moored current meters and thermographs, vol 2: Oregon continental shelf, August–September 1966, *Data Rep. 68-5*, Oregon State Univ., Corvallis.

Niiler, P. P. (1969), On the Ekman divergence in an oceanic jet, *J. Geophys. Res.*, *74*(28), 7048–7052.

Paduan, J. D., and L. K. Rosenfeld (1996), Remotely sensed surface currents in Monterey Bay from shore-based HF radar (CODAR), *J. Geophys. Res.*, *101*(C9), 669–686.

Pawlowicz, R., R. C. Beardsley, and S. J. Lentz (2002), Classical tidal harmonic analysis including error estimates in MATLAB using T_TIDE, *Comput. Geosci.*, *28*(8), 929–937.

Ramp, S. R., J. D. Paduan, I. Shulman, J. Kindle, F. L. Bahr, and F. Chavez (2005), Observations of upwelling and relaxation events in the northern Monterey Bay during August 2000, *J. Geophys. Res.*, *110*, C07013, doi:10.1029/2004JC002538.

Rosenfeld, L. K., F. B. Schwing, N. Garfield, and D. E. Tracy (1994), Bifurcated flow from an upwelling center: A cold water source for Monterey Bay, *Cont. Shelf Res.*, *14*(9), 931–964.

Rosenfeld, L. K., I. Shulman, M. Cook, J. Paduan, and L. Shulman (2009), Methodology for a regional tidal model evaluation, with application to central California, *Deep Sea Res., Part II*, *56*(3), 199–218.

Rosman, J. H., J. R. Koseff, S. G. Monismith, and J. Grover (2007), A field investigation into the effects of a kelp forest (Macrocystis pyrifera) on coastal hydrodynamics and transport, *J. Geophys. Res.*, *112*, C02016, doi:10.1029/2005JC003430.

Send, U., R. C. Beardsley, and C. D. Winant (1987), Relaxation from upwelling in the Coastal Ocean Dynamics Experiment, *J. Geophys. Res.*, *92*(C2), 1683–1698.

Woodson, C. B., et al. (2007), Local diurnal upwelling driven by sea breezes in northern Monterey Bay, *Cont. Shelf Res.*, *27*, 2289–2302.

Woodson, C. B., L. Washburn, J. A. Barth, D. J. Hoover, A. R. Kirincich, M. A. McManus, J. P. Ryan, and J. Tyburczy (2009), Northern Monterey Bay upwelling shadow front: Observations of a coastally and surface-trapped buoyant plume, *J. Geophys. Res.*, *114*, C12013, doi:10.1029/2009JC005623.

J. A. Barth and S. H. Suanda, College of Oceanic and Atmospheric Sciences, Oregon State University, 104 COAS Administration Bldg., Corvallis, OR 97331, USA. (asuanda@coas.oregonstate.edu)

C. B. Woodson, Environmental Fluid Mechanics Laboratory, Stanford University, Y2E2 Bldg., MC 4020 473 Via Ortega, Mezzanine, Green Atrium, Stanford, CA 94305, USA.